CEVE 543 Fall 2025 Assigned 1: Nonstationary Rainfall Frequency Analysis

Houston Daily Rainfall Extremes and Climate Change

Zijie (Ian) Liang

2025-10-01

Tasks

1 Task 1:Stationary GEV Analysis

1.1 Data Setup and Station Selection

1.1.a Loading Required Packages

First, load all the Julia packages I will use in this analysis:

1.1.b Loading NOAA Precipitation Data

Like previous labs, I will download and read the Texas precipitation data:

1. Check if data file already exists locally
2. Download the file if it doesn't exist

Row	stnid	noaa_id	name	state	latitude	longitude	years_of_data
	Int64	String	String	String	Float64	Float64	Int64
1	1	60-0011	CLEAR CK AT BAY AREA BLVD	TX	29.4977	−95.1599	30
2	2	60-0019	TURKEY CK AT FM 1959	TX	29.5845	−95.1869	30
3	3	60-0022	ARMAND BYU AT GENOARED BLF RD	TX	29.6345	−95.1123	31
⋮	⋮	⋮	⋮	⋮	⋮	⋮	⋮
815	815	87-0031	SECO CREEK AT MILLER RANCH	TX	29.5731	−99.4028	20
816	816	99-2048	COTULLA	TX	28.4567	−99.2183	102

Row	stnid	date	year	rainfall
	Int64	Date	Int64	Quantity…?
1	1	1987-06-11	1987	6.31 inch
2	1	1988-09-02	1988	5.46 inch
3	1	1989-08-01	1989	11.39 inch
⋮	⋮	⋮	⋮	⋮
61924	816	2016-08-20	2016	3.44 inch
61925	816	2017-09-25	2017	2.72 inch

1. Read and parse the NOAA precipitation data

Choose Houston area station for analysis.

Row	stnid	noaa_id	name	state	latitude	longitude	years_of_data	distance_km
	Int64	String	String	String	Float64	Float64	Int64	Quantity…
1	782	79-0061	HOUSTON INTER-CONT AP	TX	29.98	−95.36	48	2.44121 km
2	387	41-4362	HUMBLE	TX	30.0	−95.25	60	8.80564 km
3	6	60-0104	GREENS BYU AT MT HOUSTON PKWY	TX	29.892	−95.238	31	13.0751 km
⋮	⋮	⋮	⋮	⋮	⋮	⋮	⋮	⋮
815	807	79-0125	EL PASO	TX	31.7587	−106.484	60	1083.1 km
816	428	41-4931	LA TUNA 1 S	TX	31.98	−106.597	69	1097.22 km

1. Descriptive name for my houston area target location
2. Houston George Bush Intercontinental Airport's longitude coordinate (negative means west of Greenwich)
3. Houston George Bush Intercontinental Airport's latitude coordinate (positive means north of equator)
4. Define a function that calculates great circle distance between two lat/lon points
5. Earth's radius in kilometers (using proper units!)
6. Convert the first latitude from degrees to radians (φ is Greek phi)
7. Convert the second latitude to radians
8. Calculate difference in latitudes (Δ is Greek delta, means "change in")
9. Calculate difference in longitudes (λ is Greek lambda)
10. First part of Haversine formula: angular distance component
11. Complete the great circle distance calculation
12. Multiply by Earth's radius to get distance in kilometers
13. Start a TidierData pipeline with our stations DataFrame

14. Add distance column using `!!` to inject external variables into the TidierData expression
15. Sort the stations by distance (closest first)
16. Display the sorted stations (shows closest ones first due to ENV row limit)

1.1.c Examining the Closest Weather Station

Focus on the closest weather station that near the Houston George Bush Intercontinental Airport and look at its rainfall data:

```
Station NOAA ID: 79-0061
Station Name: HOUSTON INTERCONT AP
```

Row	stnid	date	year	rainfall
	Int64	Date	Int64	Quantity...?
1	782	1970-05-15	1970	4.23 inch
2	782	1971-12-01	1971	3.09 inch
3	782	1972-03-20	1972	6.73 inch
⋮	⋮	⋮	⋮	⋮
47	782	2016-04-17	2016	9.79 inch
48	782	2017-08-26	2017	16.3 inch

1. Filter rainfall data using `!!` to inject the external variable into TidierData

1.1.d Plotting a Time Series For the Station

Create a time series plot to see how rainfall has changed over time at this station:

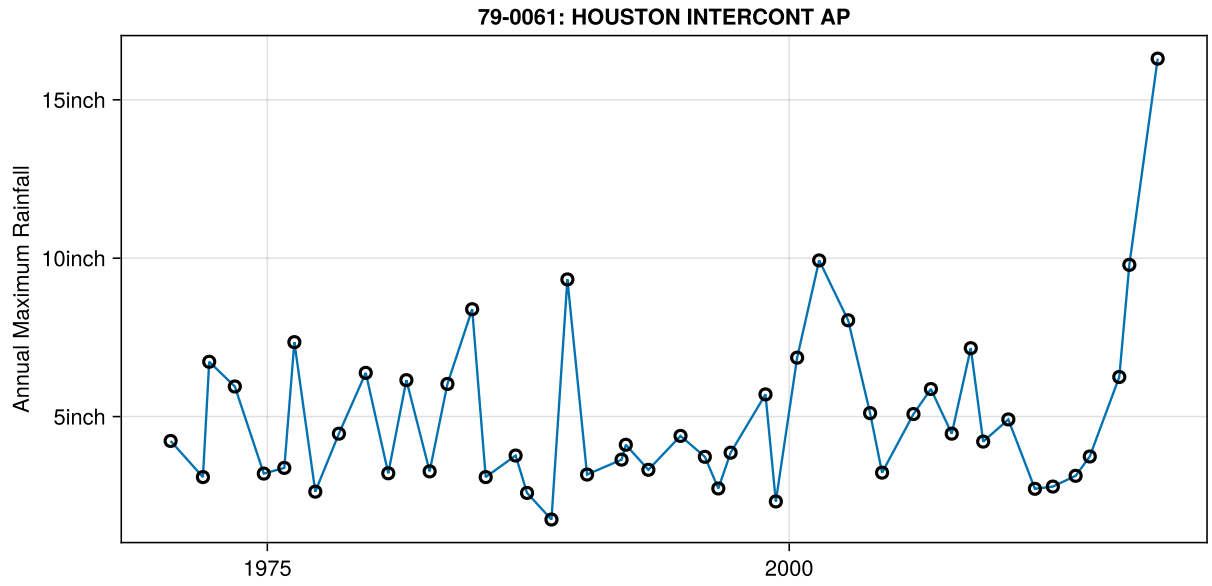

1. Use string interpolation `$()` to insert station ID and name into the plot title
2. Apply unit converter to display rainfall in inches instead of deca-inches

3. Plot using `date` column to show precise timing of annual maximum events
4. Add hollow circles with transparent fill to emphasize individual data points

1.2 GEV Fitting: Multiple Approaches

Now is the time tocompare different approaches to fitting GEV distributions to understand how estimation methods affect our results.

1.2.a MLE with Extremes.jl For Validation

First, fit a GEV distribution using maximum likelihood estimation (MLE) with `Extremes.jl` for the validation:

1. Convert rainfall data to plain numbers, removing units and missing values
2. Fit GEV distribution using maximum likelihood estimation (MLE)
3. Extract location parameter (μ) from the fitted model
4. Extract scale parameter (σ) from the fitted model
5. Extract shape parameter (ξ) from the fitted model

```
Distributions.GeneralizedExtremeValue{Float64}(μ=3.7517276015345686,
σ=1.4571087397080031, ξ=0.2509577427772232)
```

6. Create a distribution object for further analysis and plotting

1.2.b MLE Using Turning.jl With `maximum_likelihood`

Secondly, implement maximum likelihood estimation (MLE) using `Turing.jl` with [`maximum_likelihood`] workflow:

```
retcode: Success
u: 3-element Vector{Float64}:
 3.7517060773844717
 0.37645137970796505
 0.25096226384117504
```

```
Turing.jl GEV parameters (MLE):
```

Row	Parameter	Value
	String	Float64
1	Location (μ)	3.752
2	Scale (σ)	1.457
3	Shape (ξ)	0.251

1. Fit GEV distribution using maximum likelihood estimation (MLE)
2. Set up the MLE function with optimization
3. Extract location parameter (μ) from the fitted model
4. Extract scale parameter (σ) from the fitted model
5. Extract shape parameter (ξ) from the fitted model

6. Create a distribution object for further analysis and plotting

1.2.c Build a Distribution Object And Benchmark vs Extremes.jl

Check the `MLE` from Turning.jl and results from `Extreme.jl`.

Row	Method	μ	σ	ξ
	String	Float64	Float64	Float64
1	Extremes MLE	3.752	1.457	0.251
2	Turing MLE optimized	3.752	1.457	0.251

1.2.d Implement Bayesian GEV Inference using MCMC

Now I implemented the Bayesian GEV predition using MCMC. The Houston Airport(IAH) experiences annual rain depth from 1.5 to 5.0 inches mostly. When the typhoon comes, the rain depth will increase. The scale between 0.07 and 0.5 would help to control the spread of the curve. The rain depth increase slowly and change slightly in the near future so the `$\sigma$` should not be set large. The shape prior help to control the shape at the right side of the predition line.

- $\hat{R}$ values close to 1.0 (indicates chains have converged to same distribution)
- Effective sample sizes (`ess_tail` and `ess_bulk`) that are reasonably large (as close to the total number of samples as possible)

```
Parameter comparison (MLE vs posterior, 95% CI):
3×5 DataFrame
 Row │ Parameter  MLE       Post_mean  Post_low   Post_high
     │ String     Float64   Float64    Float64    Float64
─────┼──────────────────────────────────────────────────────
   1 │ μ          3.75173    3.81794   3.3657      4.32114
   2 │ σ          1.45711    1.53368   1.18266     1.97954
   3 │ ξ          0.250958   0.191364  0.0205682   0.378533
Return levels (inches): MLE vs posterior (95% CI)
5×5 DataFrame
 Row │ T_years  MLE       Posterior_mean  Posterior_low  Posterior_high
     │ Int64    Float64   Float64         Float64        Float64
─────┼──────────────────────────────────────────────────────────────────
   1 │       5   6.40551         6.48788        5.58348         7.66314
   2 │      10   8.15864         8.15679        6.83055        10.0216
   3 │      25  10.9023         10.6776         8.49687        14.1487
   4 │      50  13.4038         12.9118         9.77791        18.3236
   5 │     100  16.3643         15.5051        11.0986         23.7709
```

The table summarized the result about the parameter comparison for MLE and Bayesian posterior with 95% CI. It also reflected the return level difference that are predicted by MLE and Bayesian posterior with 85% CI.

1.3 Compare All Three Methods

Let me combine all the results together and show them in table form for visualizaiton.

```
Parameter comparison:
Return level comparison (inches):
```

Row	T_years	Extremes_MLE	Turing_MAP	Bayesian_MCMC
	Int64	Float64	Float64	Float64
1	5	6.406	6.405	6.483
2	10	8.159	8.159	8.132
3	25	10.902	10.902	10.584
4	50	13.404	13.404	12.714
5	100	16.364	16.364	15.131

Now let me combine all GEV fitting prediction line together, which included the MLE line predicted by `Turing.jl`, extreme GEV line from `Extremes.jl`, and Bayesian GEV with `Turning.jl` using MCMC.

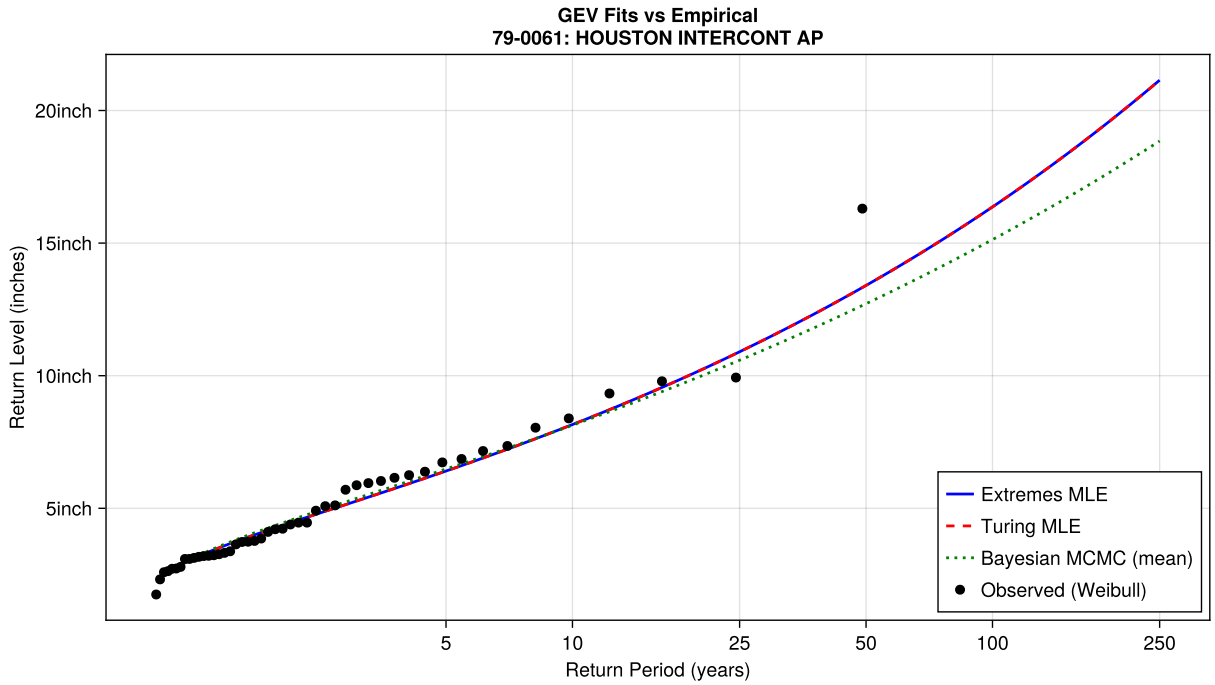

1.4 Calculate 50-year and 100-year Return Period Estimation

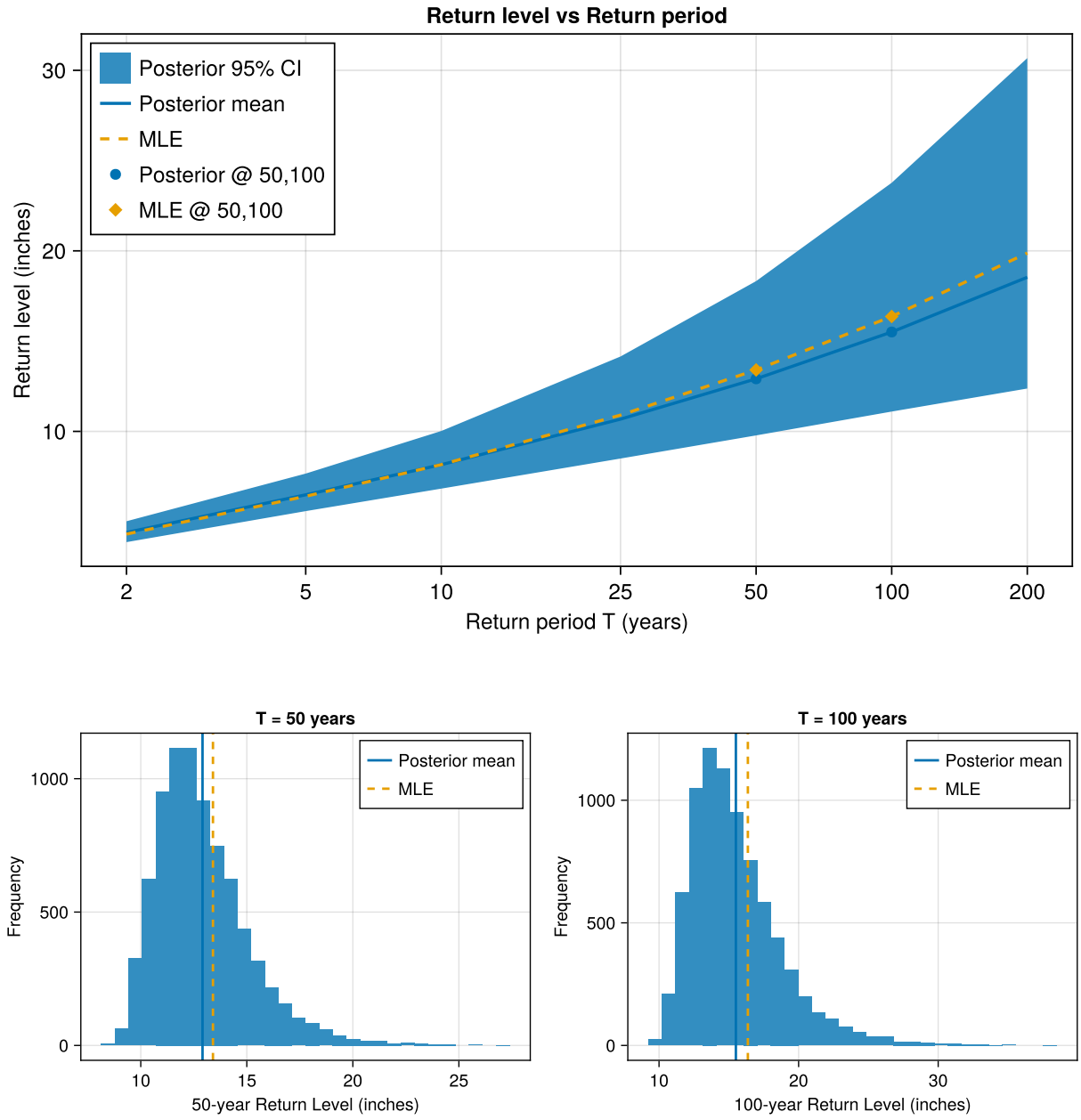

Finished task one.

2 Task 2: Multi-station Regional Analysis

2.1 Get the Nearest 4 Stations

Now is the time to check the precipitation trends for my selected station and its surrounding stations. First let me get the nearest 4 stations.

```
Nearest stations to 79-0061 (stnid=782):
```

Row	stnid	noaa_id	name	state	latitude	longitude	years_of_data	distance_km
	Int64	String	String	String	Float64	Float64	Int64	Quantity...
1	387	41-4362	HUMBLE	TX	30.0	−95.25	60	10.8366 km
2	5	60-0082	CYPRESS CK AT KUYK-ENDAHL RD	TX	30.0244	−95.4764	31	12.2614 km
3	378	41-4323	HOUSTON INDEP HTS	TX	29.8667	−95.4167	73	13.7474 km
4	6	60-0104	GREENS BYU AT MT HOUSTON PKWY	TX	29.892	−95.238	31	15.3122 km

Then I try to plot the annual precipitaion data together to check if all five stations have the same precipation data trend.

2.2 Plot The Annual Data

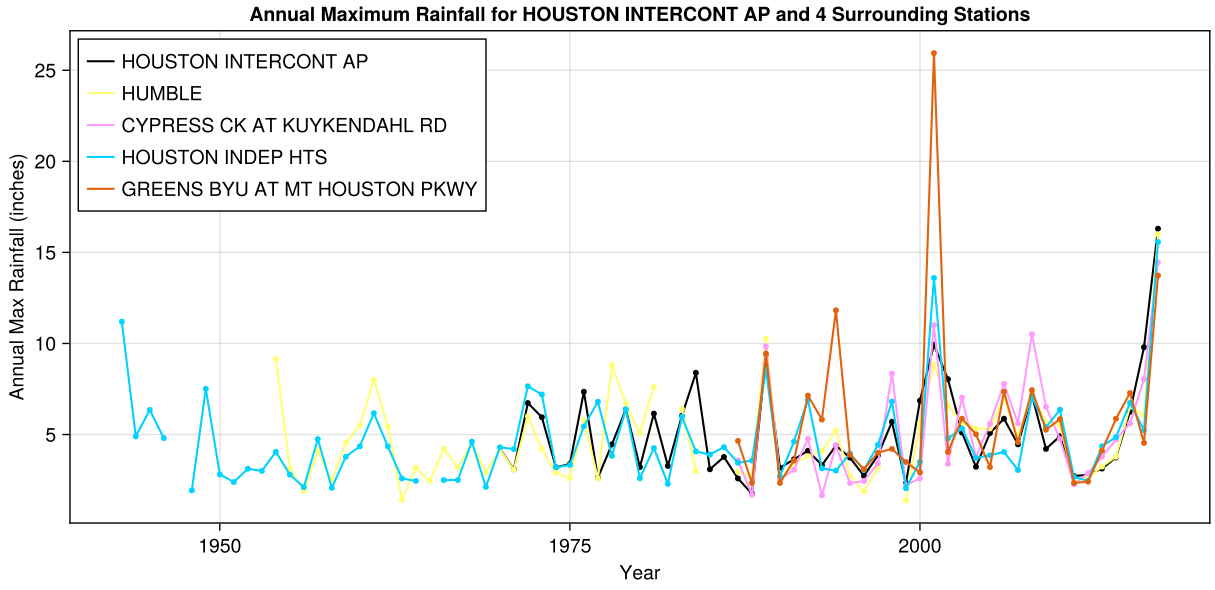

2.3 Fitting GEV to Multiple Stations

Now with the station datat from my station and the nearest 4, I could fit the GEV predition with `Extreme.jl` to them.

```
GEV parameters (MLE) for primary + 4 nearest stations:
```

Row	NOAA_ID	Name	Years	μ	σ	ξ
	String	String	Int64	Float64	Float64	Float64
1	79-0061	HOUSTON INTERCONT AP	48	3.752	1.457	0.251
2	41-4362	HUMBLE	60	3.601	1.655	0.13
3	60-0082	CYPRESS CK AT KUYKENDAHL RD	31	3.469	1.752	0.351
4	41-4323	HOUSTON INDEP HTS	73	3.44	1.311	0.273
5	60-0104	GREENS BYU AT MT HOUSTON PKWY	31	3.89	1.669	0.431

The plot and tables following shows the GEV fitting results about different stations.

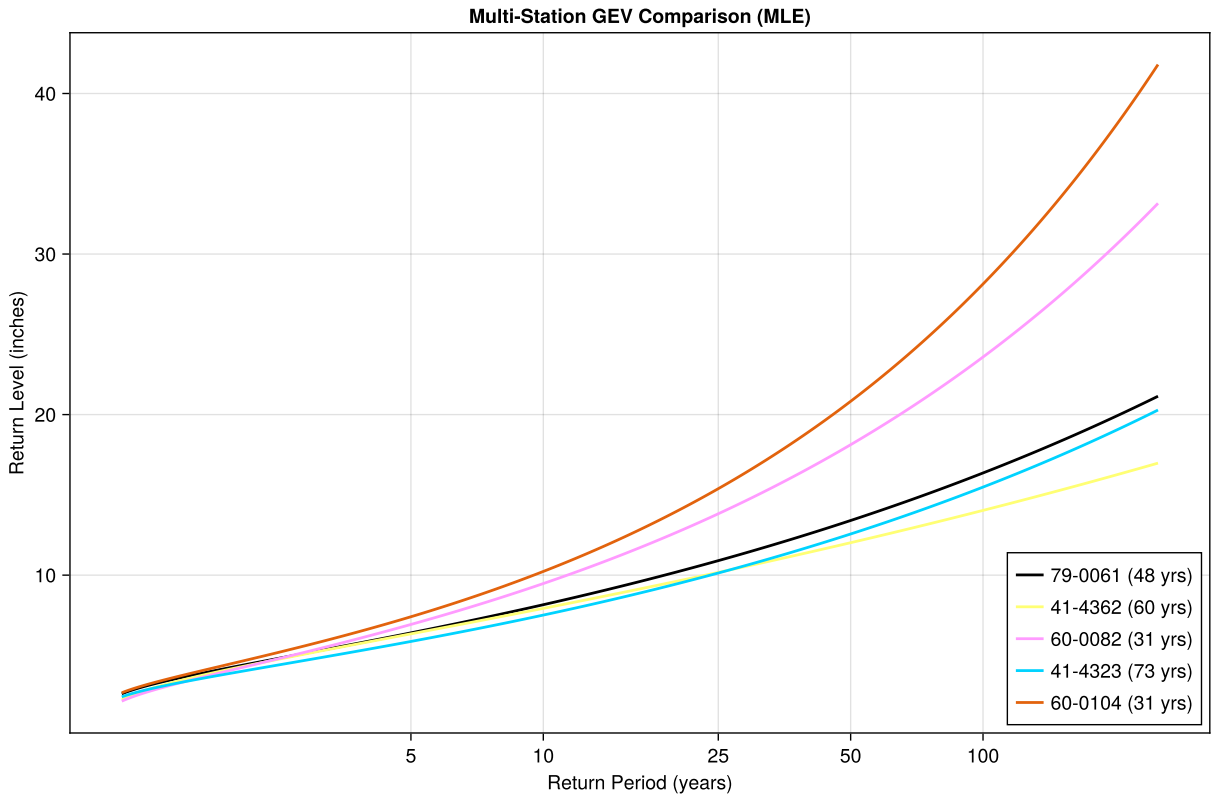

Task 2 finished.

3 Task 3: Nonstationarity Analysis

3.1 Load CO2 Data

Now let me run the nonstationarity analysis to check the reliability about my extrem value analysis.

First, I loaded the global mean CO2 concentration data, which comes from Mauna Loa (1959-2024) and from ice core reconstructions (pre-1959).

My primary satation is `Houston Internation Airport`. I loaded the data and run the potential trend signal of the CO2 data and combine them together.

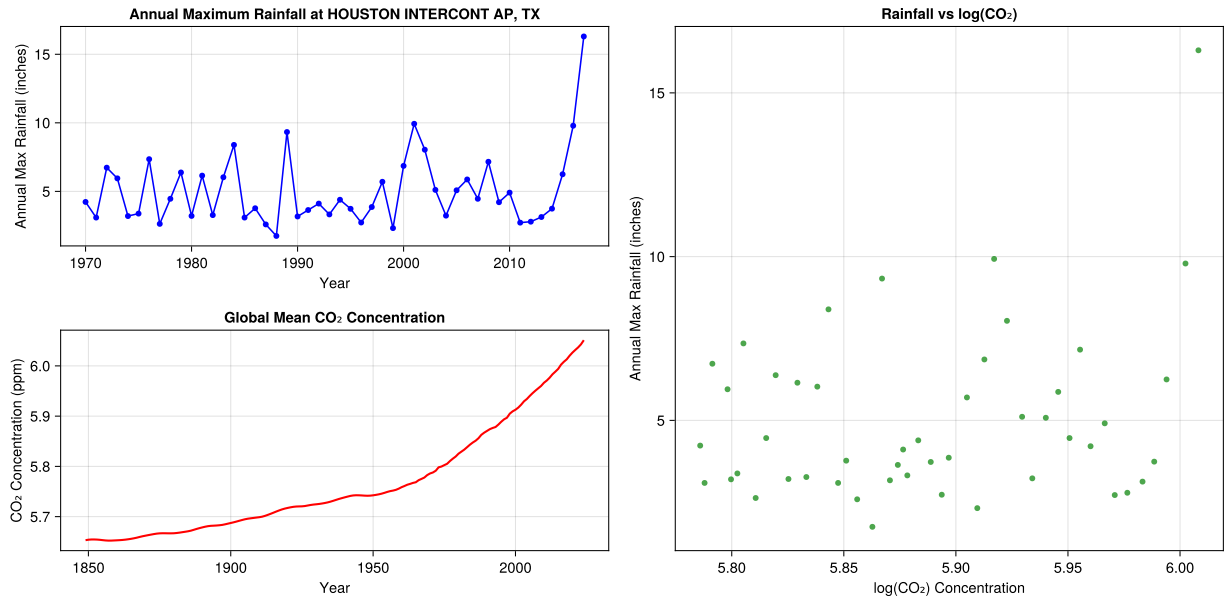

3.2 Mann-Kendall Trend Test

In order to understand the difference of the trend between the local station and the nearby station due to the inconsistent results, the nearby trends are needed to be analysised.

First, let me find the nearby data again. I will load 100 nearby data this time.

Row	stnid	noaa_id	name	state	latitude	longitude	years_of_data	distance_km
	Int64	String	String	String	Float64	Float64	Int64	Quantity…
1	782	79-0061	HOUSTON INTER-CONT AP	TX	29.98	−95.36	48	2.44121 km
2	387	41-4362	HUMBLE	TX	30.0	−95.25	60	8.80564 km
3	5	60-0082	CYPRESS CK AT KUYK-ENDAHL RD	TX	30.0244	−95.4764	31	14.6923 km
⋮	⋮	⋮	⋮	⋮	⋮	⋮	⋮	⋮
99	537	41-6680	ORANGE 9 N	TX	30.2264	−93.7394	63	156.316 km
100	310	41-3321	FRANKLIN	TX	31.0328	−96.4889	44	161.679 km

Then, I applied the Mann-Kendall test to my nearby data. I made the assumption that no serial correlation is made. The exam table included the standardized test statistic with continuity correction (S) and the two-tailed p-value (P). I used the sum of signs of all pairwise differences for the test statistic. For the hypothesis, I considered that under Null hypothesis of no trend, for `n>10`, S is normally distributed with mean 0 and variance `V = (n/18) * (n-1) * (2n+5)`.

Now apply to my actual data - testing for trends in rainfall with respect to log(CO2):

```
(114.0, 0.31521063479231004)
```

The `S value` equals to 114 and the `p-value` equals to 0.315. The S value indicates that compare with the sum of signs of all pairwise differences the data show a strong positive differences. The big `S value` reflects the strong vibration to the data, which may increase the uncertanty. The `p-value` is bigger than 0.05, indicates a rejection to the null hypothesis.

Now I applied these tests to all nearby stations and reported the results for the nearby 4 stations.

Row	stnid	noaa_id	name	state	latitude	longitude	years_of_data	mk_S	mk_pvalue
	Int64	String	String	String	Float64	Float64	Int64	Float64	Float64
1	782	79-0061	HOUSTON INTERCONTAP	TX	29.98	−95.36	48	114.0	0.315211
2	387	41-4362	HUMBLE	TX	30.0	−95.25	60	239.0	0.129028
3	5	60-0082	CYPRESS CK AT KUYKENDAHL RD	TX	30.0244	−95.4764	31	134.0	0.0237888
4	378	41-4323	HOUSTON INDEP HTS	TX	29.8667	−95.4167	73	336.0	0.110627
5	6	60-0104	GREENS BYU AT MT HOUSTON PKWY	TX	29.892	−95.238	31	69.0	0.247781

The spatial inconsistency in trend results highlights problems with single-station analysis: nearby stations show contradictory trends that are not climatologically plausible, suggesting that individual station records contain too much noise to reliably detect regional climate signals.

3.3 Two Nonstationary GEV models

Traditional extreme value analysis assumes parameters remain constant over time (stationarity). However, climate change may alter the distribution of extreme precipitation. **Nonstationarity** means the statistical properties of extremes change systematically with time or other covariates.

We'll use atmospheric CO_2 concentration as our covariate $x = \log(CO_2)$ because: - CO_2 is a primary driver of global warming - Higher temperatures can increase atmospheric moisture capacity - This may intensify extreme precipitation events

I implement two models that allow different GEV parameters to vary with CO_2 (the same as lab):

1. **Location-varying model**: Only the location parameter changes with CO_2
2. **Location and scale varying model**: Both location and scale parameters change with CO_2

Next I fit these two models to my primary station, Houston Internation Airport.

Create traceplots to visualize MCMC chain behavior for key parameters:

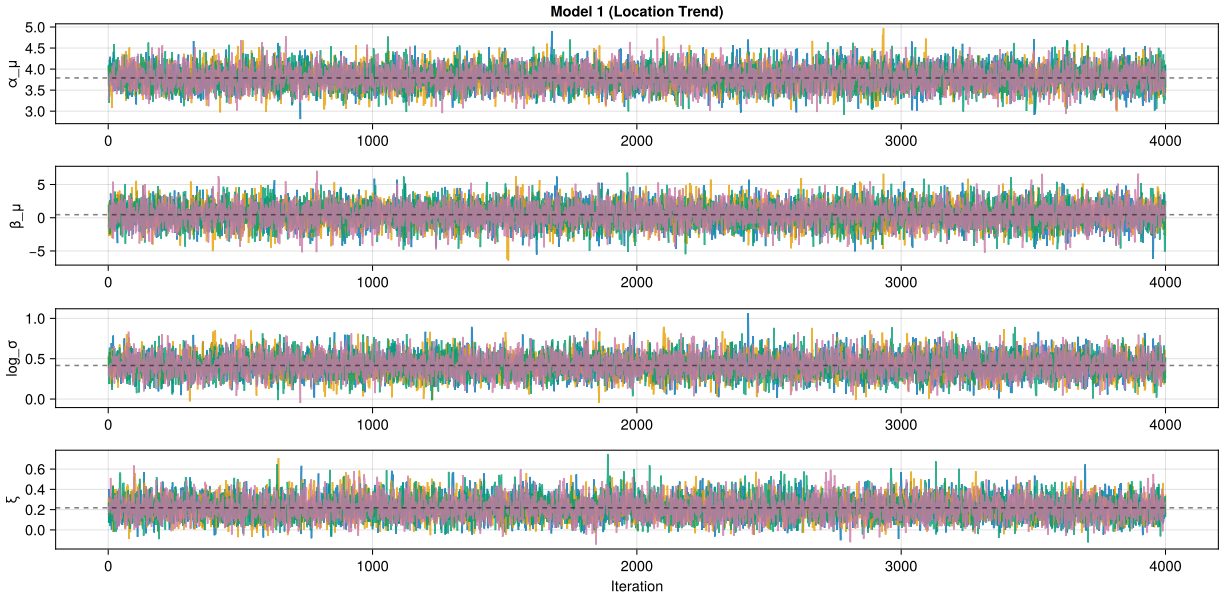

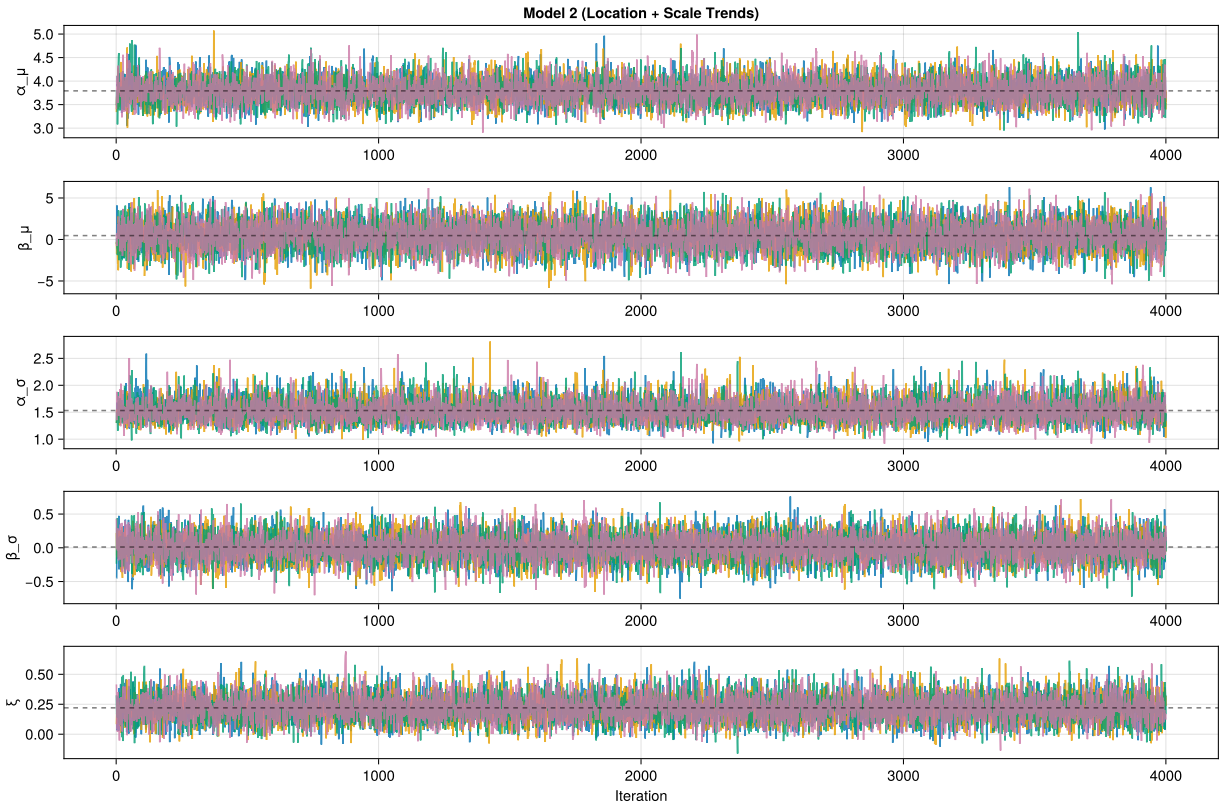

Check convergence: effective sample size should exceed 400, R-hat should be near 1.0, and traceplots should show good mixing across chains.

3.4 Extracting GEV Distributions

First, let's define functions to extract GEV distributions for any year across our two nonstationary models:

Now extract GEV distributions for both 1950 and 2025 using appropriate CO2 levels:

For the Houston Airport (IAH) station and its nearby stations, I adopted the same nonstationary GEV framework introduced earlier in the lab. My choice of covariate was the atmospheric CO_2 concentration, which acts as a long-term climate driver. CO_2 captures the monotonic global warming signal, and its rise could be linked to increases in atmospheric moisture capacity and the potential intensification of extreme rainfall. Using $\log(CO_2)$ as a covariate is therefore both physically justified and statistically useful for stabilizing inference across noisy station records.

I specified two model structures. In the `Location-trend model`, only the GEV location parameter varies with CO_2, reflecting a systematic upward or downward shift in rainfall extremes while keeping scale and shape constant. In the `Location + Scale-trend model`, both the location and scale parameters respond to CO_2, allowing the distribution to shift and stretch over time. These two specifications let us test whether climate forcing primarily shifts the center of the extremes, or also alters their spread.

3.5 Model Comparison and Uncertainty

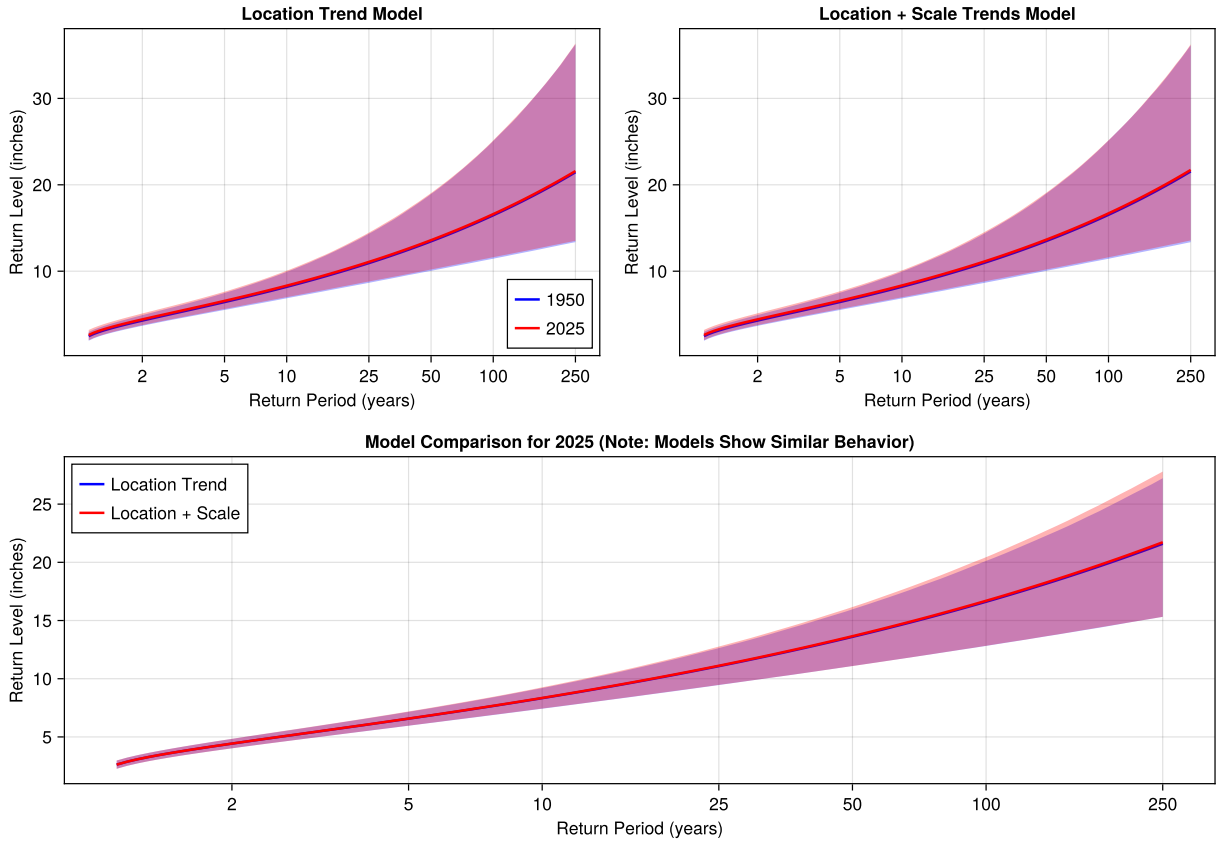

The two models show remarkably similar behavior, which is actually quite interesting - it suggests that for this dataset, allowing the scale parameter to vary with CO_2 doesn't dramatically change the return level projections. Let's examine the 100-year return period distributions more closely:

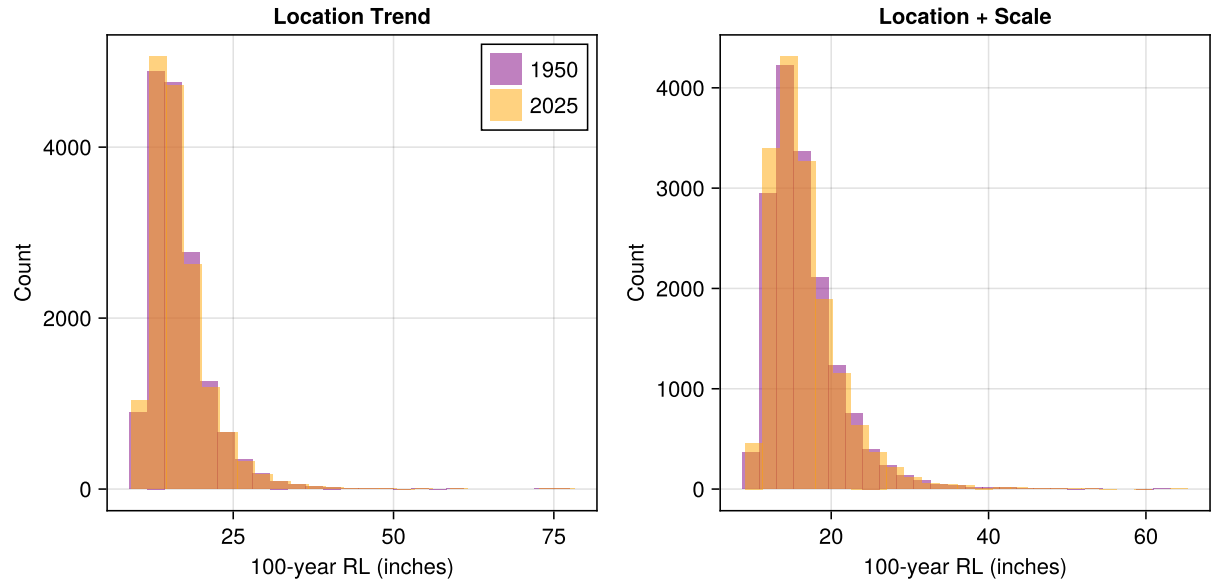

The large posterior uncertainties in single-station models, particularly for return level projections, indicate that individual stations lack sufficient data to reliably estimate trends in extreme precipitation.

For IAH and nearby stations, using log(CO_2) as a covariate captures the climate-driven intensification of extremes. Both the location-only and location+scale models show consistent results: return level curves from 1950 to 2025 diverge, with higher CO_2 linked to larger return levels. Histograms confirm that 100-year return levels shift upward, and trace plots show stable model convergence. Overall, both models indicate substantial increases in 50- to 100-year storms under future conditions, highlighting the need for nonstationary modeling in risk management and design.

4 Task 4: Regional Parameter Estimation

4.1 Regional Model Design

The large uncertainties in single-station analyses motivate regional approaches. My regional GEV model uses a simple approach where some parameters are shared regionally while others vary by station (similar to the lab).

For station i in year t:

$$Y_{i,t} \sim \text{GEV}\left(\mu_{i,t}, \sigma_i, \xi_{\text{region}}\right)$$

where:

- **Regional parameters**: β_{region} (trend) and ξ_{region} (shape) are the same for all stations
- **Station-specific parameters**: $\alpha_{\mu,i}$ (baseline location) and σ_i (scale) differ by station

The location parameter varies with the covariate $x = \log(\text{CO}_2)$:

$$\mu_{i,t} = \alpha_{\mu,i} + \beta_{\text{region}} \cdot (x_t - \log(380))$$

This approach assumes climate change affects trend and extreme value tail behavior similarly across the region, while allowing for local differences in baseline precipitation amounts and variability.

We'll select the 8 closest stations with at least 40 years of data

To analyze the data, I converted the data to a matrix, where each row corresponds to a year and each column corresponds to a station.

Then I prepared the data matrices for the hierarchical analysis:

The next step I implemented the simplified regional model:

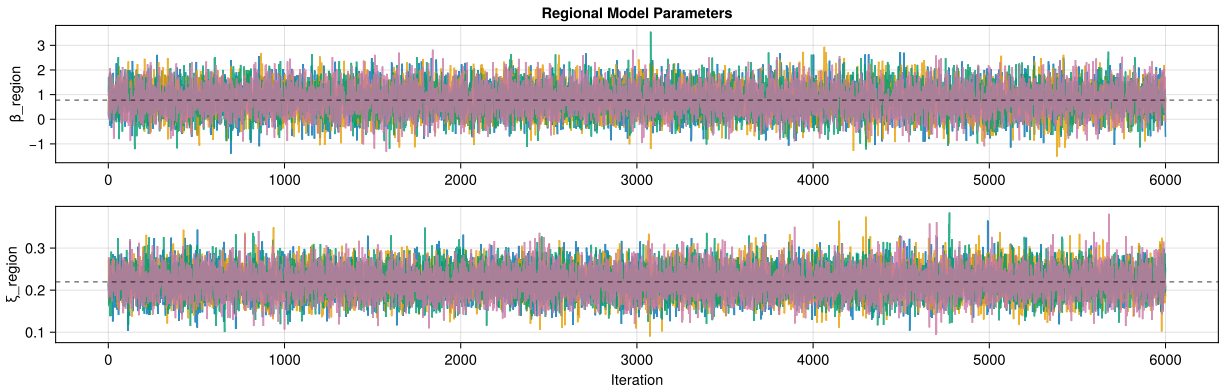

For the regional nonstationary GEV, I specify that the trend parameter and the shape parameter are shared across stations, while the baseline location and scale remain station-specific. The reasoning is that long-term climate forcing, represented by CO_2, should influence the direction and heaviness of extremes consistently across a coherent regional cluster, but baseline rainfall levels and variability differ locally due to site conditions. This structure improves identifiability by borrowing strength for trend and tail behavior, which are difficult to estimate reliably at single stations. In practice, my results show that regional pooling reduces posterior uncertainty: return-level bands for 50- and 100-year storms are narrower and trend estimates have smaller posterior standard deviations compared to single-station fits.

For the regional analysis, I defined the boundary by selecting the 8 closest stations to Houston Intercontinental Airport (IAH) with at least 40 years of data. Geographic proximity ensures that all stations experience broadly similar synoptic-scale climate drivers, such as Gulf moisture and tropical storm influences, while the data-length criterion guarantees sufficient record depth for stable estimation. This balance avoids including short or gappy records that inflate uncertainty. At the same time, limiting the region to nearby stations reduces the risk of pooling across climatologically inconsistent areas. he spatial Mann–Kendall tests also highlighted inconsistencies in single-station trends, reinforcing the value of pooling only across stations within a climatologically coherent neighborhood.

4.2 Comparing Regional vs Single-Station Approaches

Compare how the regional model performs versus the single-station nonstationary models for our primary station for the 50-year return levels.

```
24000-element Vector{GeneralizedExtremeValue{Float64}}:
 Distributions.GeneralizedExtremeValue{Float64}(μ=3.498241407566658,
σ=1.6682429846368692, ξ=0.20836596028280543)
 Distributions.GeneralizedExtremeValue{Float64}(μ=3.625799214242691,
σ=1.692013774425666, ξ=0.2177353866022649)
 Distributions.GeneralizedExtremeValue{Float64}(μ=3.6553856445224167,
σ=1.3218331524812528, ξ=0.17653929581337235)
 Distributions.GeneralizedExtremeValue{Float64}(μ=3.533975949217747,
σ=1.665216483226898, ξ=0.19486479672972948)
 Distributions.GeneralizedExtremeValue{Float64}(μ=3.676851474205039,
σ=1.4632256488941986, ξ=0.2202951224327875)
 Distributions.GeneralizedExtremeValue{Float64}(μ=3.624031030158405,
σ=1.4633410586628552, ξ=0.2251112893041901)
```

```
 Distributions.GeneralizedExtremeValue{Float64}(μ=3.701067462750299,
σ=1.4027891180633576, ξ=0.207354797162331)
 Distributions.GeneralizedExtremeValue{Float64}(μ=3.4036390577506936,
σ=1.4341778998394348, ξ=0.19247738545663381)
 Distributions.GeneralizedExtremeValue{Float64}(μ=3.52466188132324,
σ=1.4147878978381057, ξ=0.20164001614473834)
 Distributions.GeneralizedExtremeValue{Float64}(μ=3.8246043638951597,
σ=1.5025437086990672, ξ=0.23464086490399005)
 ⋮
 Distributions.GeneralizedExtremeValue{Float64}(μ=3.437594409369996,
σ=1.152947345553533, ξ=0.21053417625873655)
 Distributions.GeneralizedExtremeValue{Float64}(μ=4.028305759514393,
σ=1.6960978511340667, ξ=0.226211384156977)
 Distributions.GeneralizedExtremeValue{Float64}(μ=3.284850686842242,
σ=1.262456119675458, ξ=0.24145230358247263)
 Distributions.GeneralizedExtremeValue{Float64}(μ=3.616097268184011,
σ=1.588298075940779, ξ=0.20138738807176526)
 Distributions.GeneralizedExtremeValue{Float64}(μ=3.71906783323945,
σ=1.4664694781105585, ξ=0.22389749953461374)
 Distributions.GeneralizedExtremeValue{Float64}(μ=3.5672794492891677,
σ=1.4589091506987466, ξ=0.22789647357155948)
 Distributions.GeneralizedExtremeValue{Float64}(μ=3.6017841134358255,
σ=1.5208358256201087, ξ=0.22077673028239134)
 Distributions.GeneralizedExtremeValue{Float64}(μ=3.442194483878525,
σ=1.4070585018079873, ξ=0.2062929208504614)
 Distributions.GeneralizedExtremeValue{Float64}(μ=3.4606502438448254,
σ=1.5105041488917017, ξ=0.21086195876405295)
```

Then generate the return level curves for the comparesion.

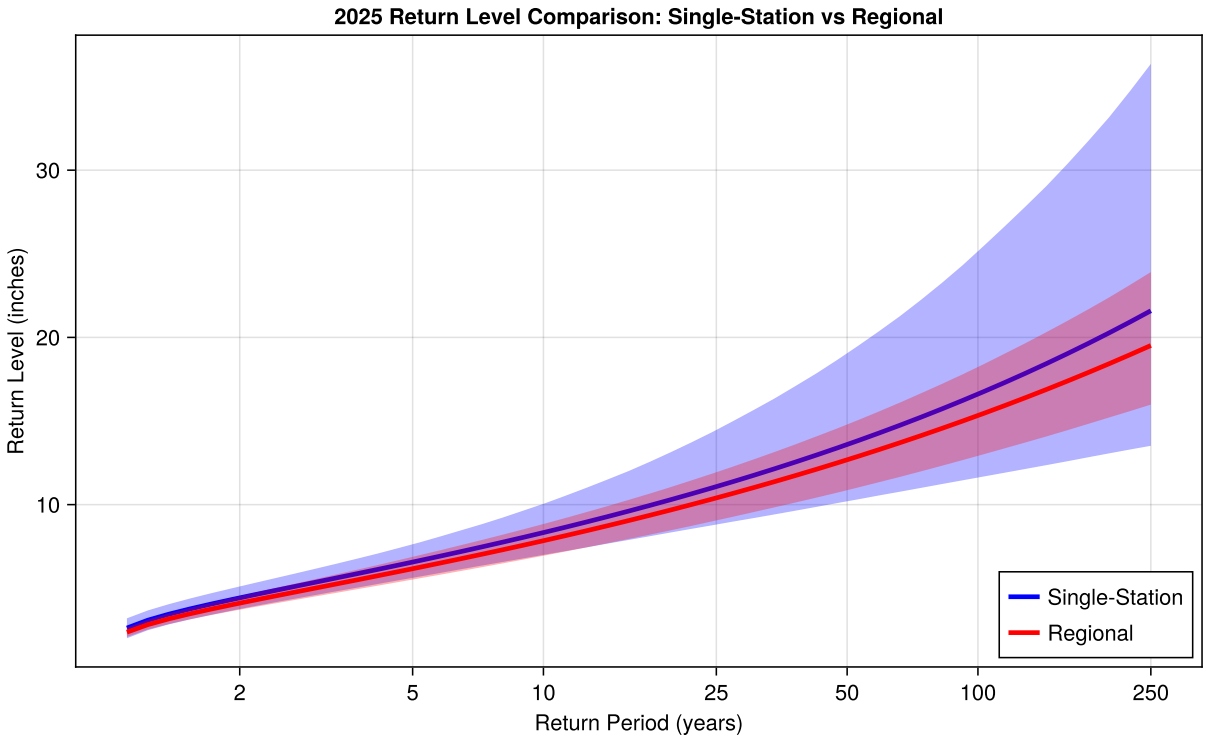

Next, compare the parameter uncertainty for different scales.

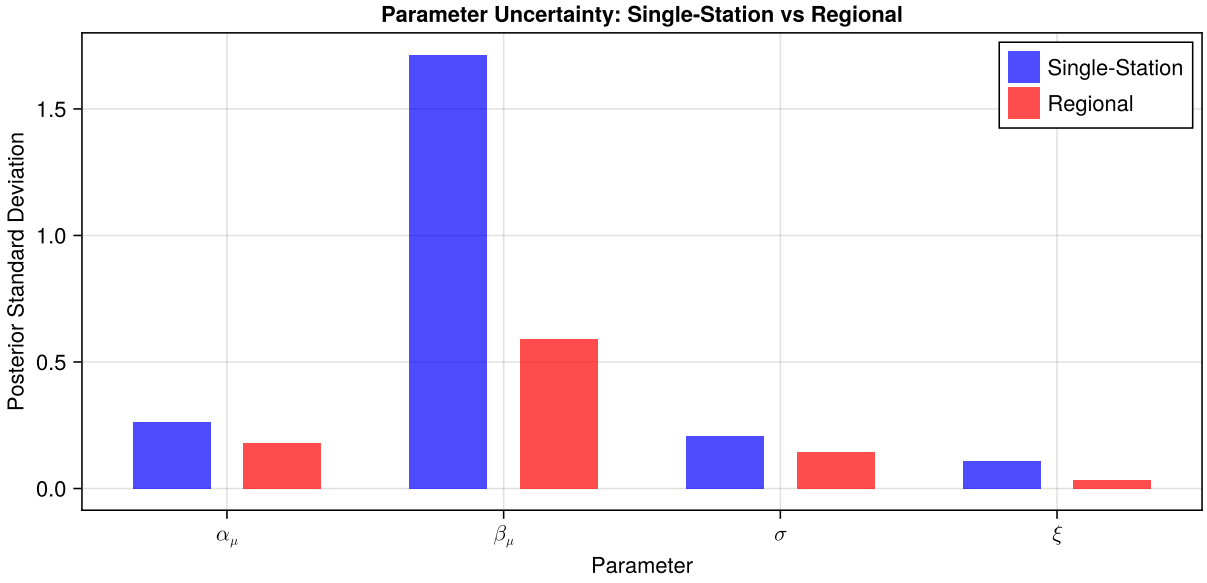

Generate the 50 years return level uncertainty plots.

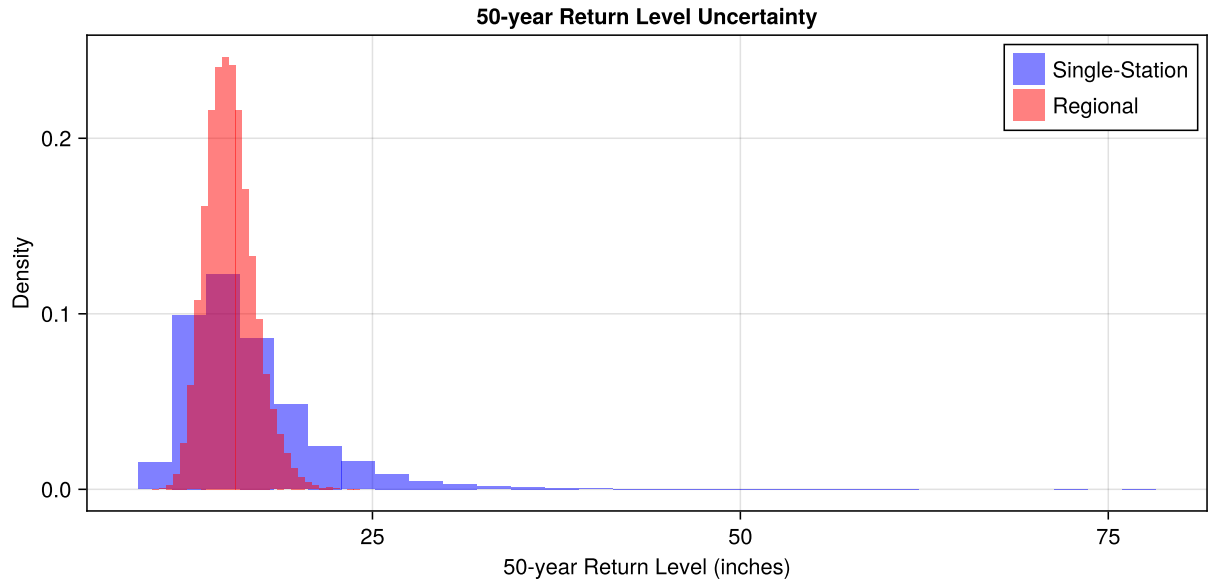

Trend estimates compare between the single-station and regional approaches:

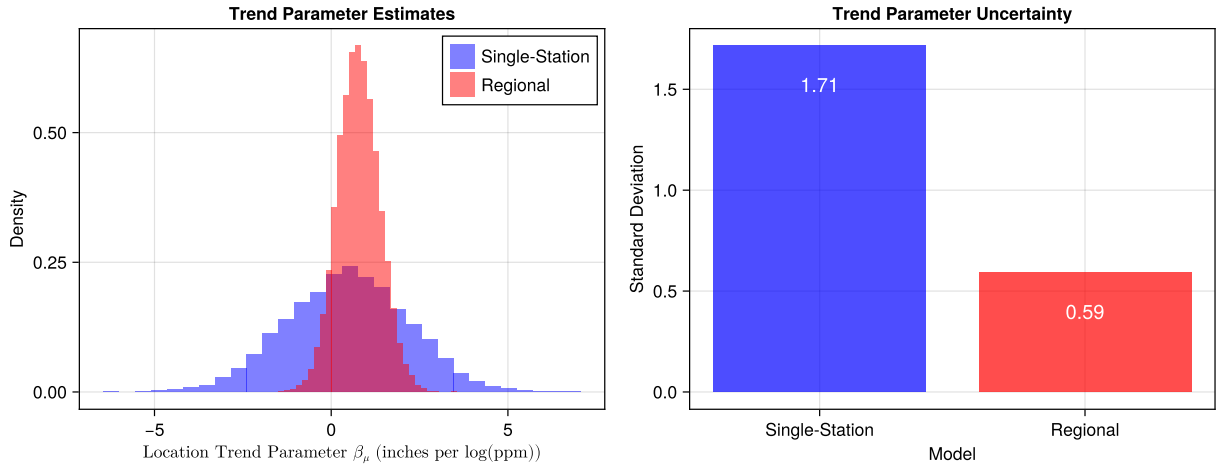

The regional approach appears to provide a somewhat more precise estimate of the trend parameter. This improved precision occurs because by pooling the shape parameter and constraining the station-specific parameters, I can get better estimates of the other model components, which in turn help constrain our trend estimate. This demonstrates how regional modeling can sharpen parameter estimates through better overall model specification.

5 Task 5: Communication

5.1 Question 1

The belief that 50 years of multiple station data are sufficient to exam how uncertainty compounds in extreme value estimation. Single-station maximum likelihood methods produce point estimates with deceptively narrow confidence intervals, yet their reliability is undermined by short and noisy records. In my analyses at Houston Intercontinental Airport, the Bayesian approach explicitly quantified parameter

uncertainty by generating full posterior distributions, revealing that 50- and 100-year return levels carried wide credible intervals that MLE alone could not capture. Extending the single station to a regional Bayesian framework further reduced variance by pooling information across nearby climatologically coherent stations. By sharing trend and shape parameters regionally while retaining site-specific baselines and scales, the model produced tighter return-level bands and more compact histograms of return levels, without biasing the central estimate. The multi-station test demonstrates that climate-informed Bayesian regional modeling does not add unnecessary complexity but instead stabilizes design values and reduces noise-driven overestimation.

5.2 Question 2

Evidence from both the single-station and regional analyses shows that assuming stationarity risks underestimating future extremes. At IAH, nonstationary GEV models with (CO_2) as a covariate revealed clear upward shifts in return level curves from 1950 to 2025, with the 100-year return level distributions moving several inches higher under rising CO_2. Even though `location-only` and `location+scale` models produced similar mean projections, their consistent divergence from stationary fits demonstrates that climate forcing cannot be ignored. Prior specification also matters. Weakly informative priors on the scale trend prevented overfitting while still allowing the model to detect credible increases in variability. Posterior diagnostics also confirmed well-mixed chains and stable inference. For critical infrastructure, such underestimation translates into increased failure risk, higher life-cycle costs, and cascading social impacts when systems designed to past climate baselines face intensifying rainfall extremes. Nonstationary Bayesian models therefore offer not just academic refinement, but a practical safeguard against underbuilding in the face of documented climate-driven change.